Lab on a Chip

Miniaturisation for chemistry, biology & bioengineering

www.rsc.org/loc

Volume 8 | Number 2 | February 2008 | Pages 181–368

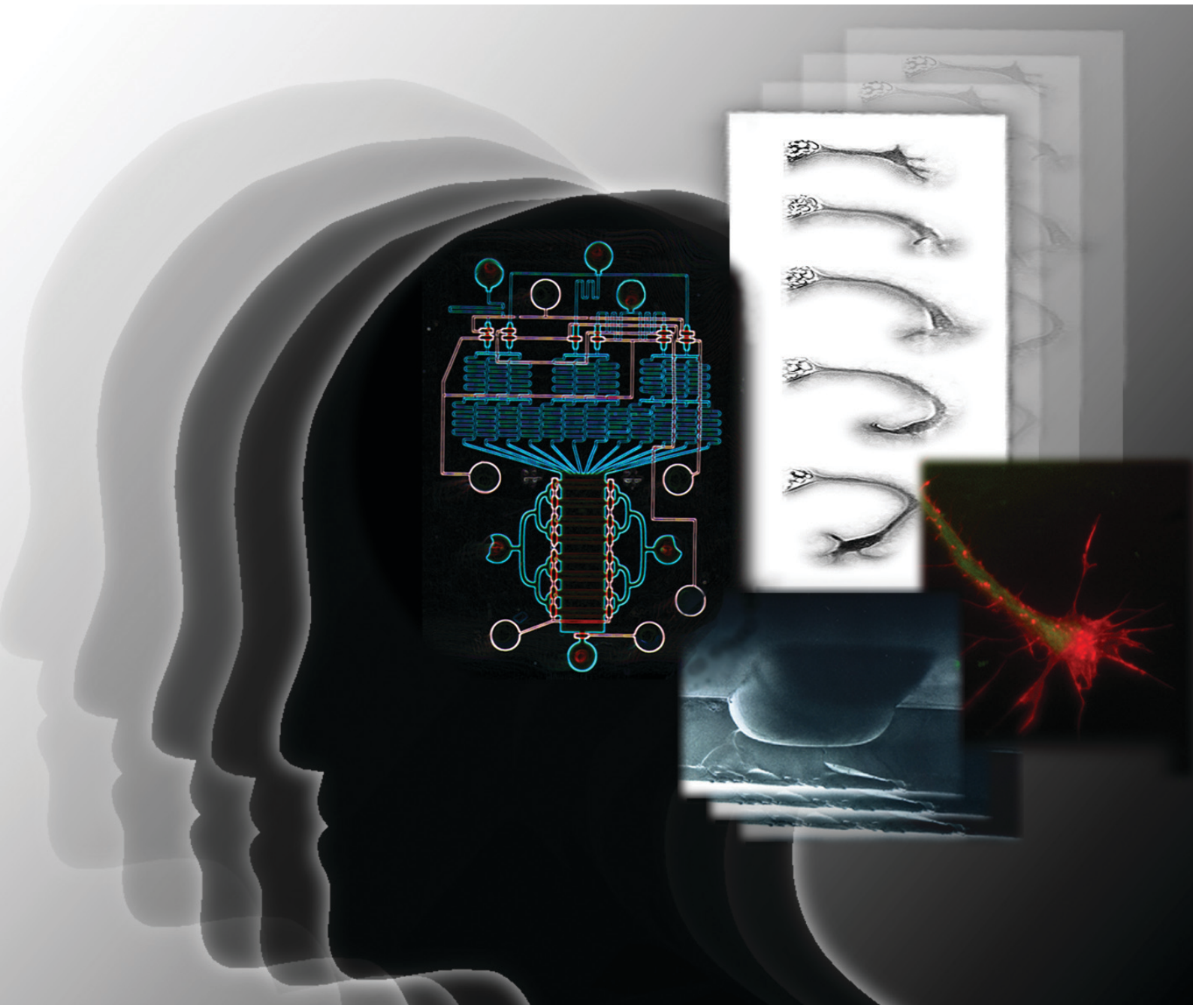

ISSN 1473-0197

RSC Publishing

1473-0197(2008)8:2;1-1

A microfluidics-based turning assay reveals complex growth cone responses to integrated gradients of substrate-bound ECM molecules and diffusible guidance cues†

C. Joanne Wang,‡[ac] Xiong Li,‡[ac] Benjamin Lin,[a] Sangwoo Shim,[bc] Guo-li Ming[bc] and Andre Levchenko*[ac]

Received 11th September 2007, Accepted 4th December 2007
First published as an Advance Article on the web 4th January 2008
DOI: 10.1039/b713945d

Neuronal growth cones contain sophisticated molecular machinery precisely regulating their migration in response to complex combinatorial gradients of diverse external cues. The details of this regulation are still largely unknown, in part due to limitations of the currently available experimental techniques. Microfluidic devices have been shown to be capable of generating complex, stable and precisely controlled chemical gradients, but their use in studying growth cone migration has been limited in part due to the effects of shear stress. Here we describe a microfluidics-based turning-assay chip designed to overcome this issue. In addition to generating precise gradients of soluble guidance cues, the chip can also fabricate complex composite gradients of diffusible and surface-bound guidance cues that mimic the conditions the growth cones realistically counter *in vivo*. Applying this assay to *Xenopus* embryonic spinal neurons, we demonstrate that the presence of a surface-bound laminin gradient can finely tune the polarity of growth cone responses (repulsion or attraction) to gradients of brain-derived neurotrophic factor (BDNF), with the guidance outcome dependent on the mean BDNF concentration. The flexibility inherent in this assay holds significant potential for refinement of our understanding of nervous system development and regeneration, and can be extended to elucidate other cellular processes involving chemotaxis of shear sensitive cells.

Introduction

During both embryonic development and regeneration following nerve injury, extending axons must navigate to the appropriate targets in a highly directed manner. This path-finding process is mediated by the enlarged tip of an axon, the growth cone, which senses complex gradients formed by diverse extra-cellular guidance cues and integrates their inputs throughout extensive migration paths. In particular, two commonly encountered forms of guidance cues—diffusible factors secreted by the cells in the growth cone microenvironment and surface-bounded guidance cues presented either on the cell surface or on the extra-cellular matrix (ECM)[1,2]—are processed by the navigating growth cones in a still largely uncharacterized fashion.

Several *in vitro* assays have been developed to study growth cone behavior in the presence of exogenously added gradients of molecular cues. The micropipette ejector has been by far the most extensively used assay to study growth cone guidance by diffusible cues.[3–7] It functions by periodically ejecting fixed amounts of chemical solutions *via* a micropipette tip near a growth cone, producing approximately exponentially shaped gradients. Variations in the generated gradients can be achieved by either varying the distance of the pipette tip from the growth cone or changing the concentration of the loaded stimulant.[3] However, regardless of the application details, the slope and the mean concentration of the guidance cue can only be changed concomitantly, effectively limiting one's ability to investigate how these parameters individually regulate growth cone responses. A more recent chemotaxis assay based on passive diffusion in collagen gels has been proposed by Rossoff *et al.*[8] This assay system, capable of controlling the shape, value and mean concentration of a gradient, has been utilized to demonstrate the sensitivity of axons from dorsal root ganglion (DRG) explants to nerve growth factor (NGF) gradients. However, the gradient generated in this approach is present during neurite initiation, making it difficult to determine whether the asymmetric distribution of axons is due to uneven neurite initiation or due to directed axon turning. Furthermore, this method does not allow tracking of the molecular dynamics within single growth cones, *e.g.*, by using fluorescent tags or dyes. Attempts have also been made to analyze axon guidance in response to insoluble cues, mostly using 'stripe assays', in which directive molecules are patterned in stripes intermittent with permissive coatings.[9,10] Recently, two groups have demonstrated the use of a photo-immobilization technique[11] and a microfluidics device[12] to generate a more precise surface-bound gradient.

[a]*Department of Biomedical Engineering and Whitaker Institute of Biomedical Engineering, The Johns Hopkins University School of Medicine, Baltimore, MD 21218, USA*
[b]*Department of Neurology, The Johns Hopkins University School of Medicine, Baltimore, MD 21218, USA*
[c]*Institute of Cell Engineering, The Johns Hopkins University School of Medicine, Baltimore, MD 21218, USA. E-mail: alev@jhu.edu; Fax: +1 410 516 6240; Tel: +1 410 516 6241*
† Electronic supplementary information (ESI) available: Supplemental methods, figures and legends. See DOI: 10.1039/b713945d
‡ These authors contributed equally.

These assay systems have unquestionably facilitated the understanding of the molecular and cellular mechanisms underlying growth cone guidance. However, they also have probably yielded a highly simplified picture of the guidance process, due to inherent limitation of the analysis of responses to a single directive cue. Under physiological conditions, the navigation of growth cones is regulated by the concerted action of diffusible and surface-bound cues. More realistic assay systems which can evaluate the effect of combinatorial cues on growth cone turning are currently unavailable. A viable solution to this unmet need is the use of microfluidic devices. Typically constructed of optically transparent materials,[13] such as polydimethyl siloxane (PDMS) and glass, microfluidic devices are compatible with any type of optical microscopy. The generated gradients of single or multiple factors can be of arbitrary shapes and varying spatial-temporal characteristics, allowing unprecedented control over the cell-culture microenvironment. In certain types of fluidic network design, a steady-state gradient generated by convective flow can be maintained for as long as an experiment requires.[14,15] These types of devices have already been used to assay chemotaxis in neutrophils,[16] but they are not directly applicable to assaying growth cone guidance. Unlike neutrophils or endothelial cells, neurons physiologically reside in tissues free of continuous fluid flows. Therefore, culturing neurons in a microfluidic chamber with an unnaturally high shear stress level can markedly decrease axon survival rates and effectively nullify the advantages of a microfluidic system. To eliminate the effect of shear, a diffusion-based method for generating a stable linear gradient has been recently demonstrated.[17] However, the method is not applicable to large ligands, as it would take hours for the gradient to equilibrate across the length scale of an axon by diffusion alone, thus making tracking of turning initiation difficult.

In this report we describe the development of a microfluidics-based assay system enabling the analysis of growth cone responses to simple or composite gradients of precisely generated and aligned surface-bound and diffusible cues. The 'composite-gradient generator' device we designed remedies commonly observed axonal retraction in flow by incorporating micro-well structures to shield neurons from shear stress. Moreover, this device incorporated on-chip pneumatic valves to control the topology of the fluidic channel networks, allowing a single device to generate multiple gradients of different shapes and moieties. We used *Xenopus* embryonic spinal neurons as a model system and applied the device to investigate how the polarity of growth cone guidance is regulated by gradients of surface-bound laminin and diffusible BDNF (brain-derived neurotrophic factor) gradients. In addition to showing that growth cones can sense shallow linear BDNF gradients, we observed that the turning of growth cones in a BDNF gradient alone was independent of the local average BDNF concentration, whereas in combined gradients of laminin and BDNF the precision and directionality of the turning was highly dependent on BDNF concentration. These unexpected observations suggest that the described device can modify and extend our understanding of the complex growth cone guidance mechanisms.

Experimental

PDMS device fabrication

The dual-layer microfluidic device (Fig. 1) was made of two layers of PDMS (GE RTV) using soft lithography.[13] The master mold for the bottom, fluidic layer had a 30 μm-thick SPR-220 relief with rounded edges. The mold was spin-coated with ~150 μm-thick layer of PDMS prepolymer (20 monomer : 1 curing agent), which was cured in the standard pre-bonding condition. The master mold for the top, control layer had a 40 μm-thick SU-8 relief. It was used to make a ~5 mm-thick PDMS (5 monomer : 1 curing agent) cast that was cut into individual chips. The inlets on this layer

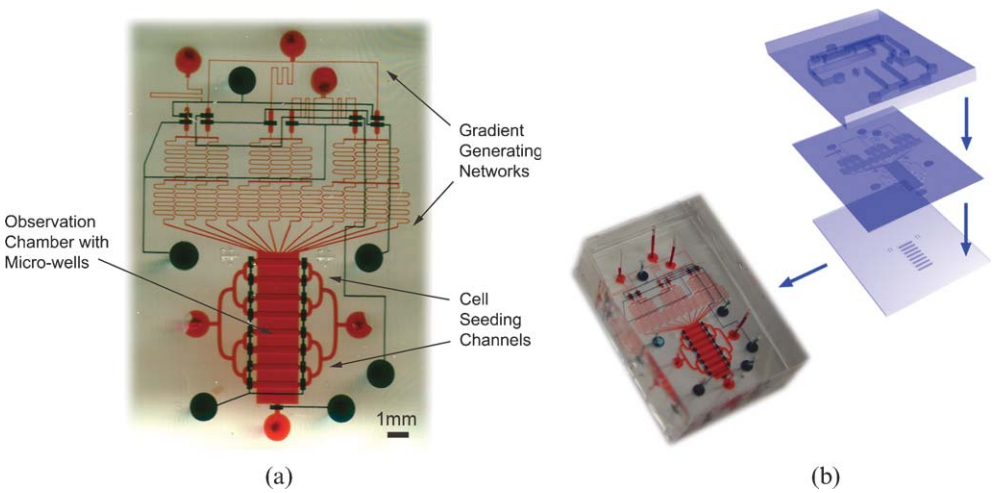

Fig. 1 The composite-gradient generator is composed of two parts: a custom microfabricated PDMS chip and a glass coverslip. (a) The PDMS chip has two layers: the bottom fluidic layer (red) contains a gradient generating network, a symmetric cell seeding network and a chemotaxis observation chamber; the top layer (blue) contains pneumatic control valves which can turn on or off the flow in the specified fluidic channels on the bottom layer. The glass coverslip is wet-etched with an array of micro-wells (darker red). (b) The three-dimensional relationship between all the layers is schematically demonstrated on the right panel. The actual device is filled with food dyes to facilitate visualization.

were drilled using a syringe tip. The chips were then aligned manually using a stereoscope (Carl Zeiss Stemi DV4) and placed on top of the partially cured PDMS layer on the bottom fluidic layer wafer. After another partial curing, monolithic two-layer PDMS chips were peeled off the master mold, had the remaining inlets drilled, were aligned, and placed on top of the micro-well containing glass coverslips. After the final oven curing, PDMS chips were formed. (This process will be described in detail in the Integration section.)

Glass micro-well machining by wet etching

#1.5 glass coverslip (~170 μm–20 μm thick, Fisher) was thermally evaporated with layers of chromium/gold (300A/1000A), and patterned with SPR-220 positive photoresist. Gold etchant and chromium etchant were then used to etch away the exposed metal areas that were not protected by the photoresist. With its back protected using etching masking tape, the glass coverslip was wet etched in HF : HNO_3 : H_2O (20 : 14 : 66 by percentage) for 10 minutes. The etching rate was 10 μm per minute, yielding a total well depth of 100 μm. The etching masking tape was removed by manual peeling, then the masking layers were sequentially removed with acetone, gold etchant, and chromium etchant. The finished product was rinsed with isopropanol and DI water, and dried with compressed air.

Integration of PDMS device and glass micro-wells

The dual layer PDMS device was manually aligned and hermetically sealed with the etched glass coverslip with the aid of an inspection scope. This process is typically accomplished in seconds and is as straightforward as bonding the device to an unetched glass coverslip. The PDMS-glass reversible bond was then reinforced by heating in a 90 °C oven overnight. The resulting microchannels were found to withstand up to 7 psi of pressure without bursting or leaking fluid. After use, the PDMS chips were either disposed of or recycled using the following procedure. The PDMS chip and the coverslip were separated from each other, both washed in diluted bleach, followed by Alconox solution and 100% ethanol. Chips were then dried with sterile filtered compressed air, and then stored away in sealed Petri dishes.

Xenopus spinal neuron culture

Embryonic *Xenopus* spinal neurons were prepared from the neural tube tissues of one-day-old embryos by methods described previously.[18] Unless otherwise noted, the surface of the microfluidic device was sequentially coated before cell loading with poly-D-lysine (PDL, Sigma, MO; 0.5 mg mL^{-1} in H_2O) at room temperature for 2 h and mouse-laminin (BD Bioscience, CA; 20 μg mL^{-1} in PBS) or laminin conjugated with rhodamine at room temperature overnight. Rhodamine–laminin was conjugated per manufacturer's instructions (Pierce Weightless Dye Kit). Channels were then purged with culture media (49.5% (v/v) L-15 Leibovitz medium (GIBCO, MD), 49.5% (v/v) Ringer solution (115 mM NaCl, 2 mM $CaCl_2$, 2.6 mM KCl, and 10 mM HEPES [pH 7.6]) and 1% (v/v) penicillin/streptomycin (GIBCO, MD)). For a typical experiment, 4 neural tubes were usually dissected and resuspended in 10 μL. Neurons were loaded into the microfluidic device *via* cell inlet ports using a gel-loading micropipette tip. Loading is usually finished within 1 or 2 minutes, using a flow rate of ~1 μL min^{-1}. Approximately 40–100 neurons were seeded per well. The culture was incubated at room temperature (20 °C–22 °C) for 6 h before gradient stimulation.

Generation of a substrate-bound N-shaped laminin gradient in the composite-gradient generator

We first uniformly coated the glass surface with positively charged PDL (0.5 mg mL^{-1}) at room temperature for 2 h, then initiated the stream carrying rhodamine–laminin (20 μg mL^{-1}) from the inlet II (Fig. 2) and the streams carrying 0.03% BSA (wt%, equivalent to 300 ug mL^{-1}) from the inlets I and III (Fig. 2) at a volumetric flow rate of 680 nL min^{-1}. The valve configuration utilized to generate the N-shaped gradient of laminin in solution was shown in the left panel of Fig. 2.

Valve 3 was activated to prevent inter-circulation among the cell introduction network. Rhodamine–laminin and BSA were immobilized onto the charged glass surface by non-specific adsorption overnight. BSA was carried in the balancing streams for blocking the non-laminin surface binding sites, otherwise, even low amounts of laminin would completely saturate the surface after a sufficient period of time.

Generation of a linear soluble BDNF gradient in the composite-gradient generator

After the substrate was coated with uniform laminin or N-shaped laminin gradient, reservoirs of BDNF-containing saline (Promega, Madison, WI; 50 ng mL^{-1}) and BDNF-deficient saline were connected to inlets II and III, respectively (Fig. 2), prior to cell introduction. Valves 1, 2 and 4 were closed at this time to prevent the entry of BDNF into the network. After neurons were loaded and in-chip cultured for 6 h, we initiated the turning assay by closing valves 3, 5 and 6 and opening valves 1, 2 and 4 (Fig. 2, right panel). In this way, we reconstructed the microchannels so that only the middle pyramidal network was in use. A hydraulic pressure differential of 0.054 psi was applied between the inlets (II and III) and the outlet (VI), generating a volumetric flow of 56.7 nL min^{-1} in the observation chamber. By monitoring the intensity of a fluorescent tracer (Alexa 488, Molecular Probes) mixed with the BDNF-containing saline, we were able to confirm the balance between the inlet streams and the linear \-shaped gradient of BDNF generated in the observation chamber.

Growth cone turning assay and statistical analysis of data

The reference axis for all our angles is the line perpendicular to the direction of flow. The initial angle is defined as the angle between distal 20 μm segment of the neurite (or the so called initial direction) and the reference axis before flow is triggered. Consequently, the turning angle is defined as the angle between initial direction of neurite extension and the subsequent line connecting the growth cone positions prior to and after the one-hour assay. Fig. 1A in the ESI† illustrates the

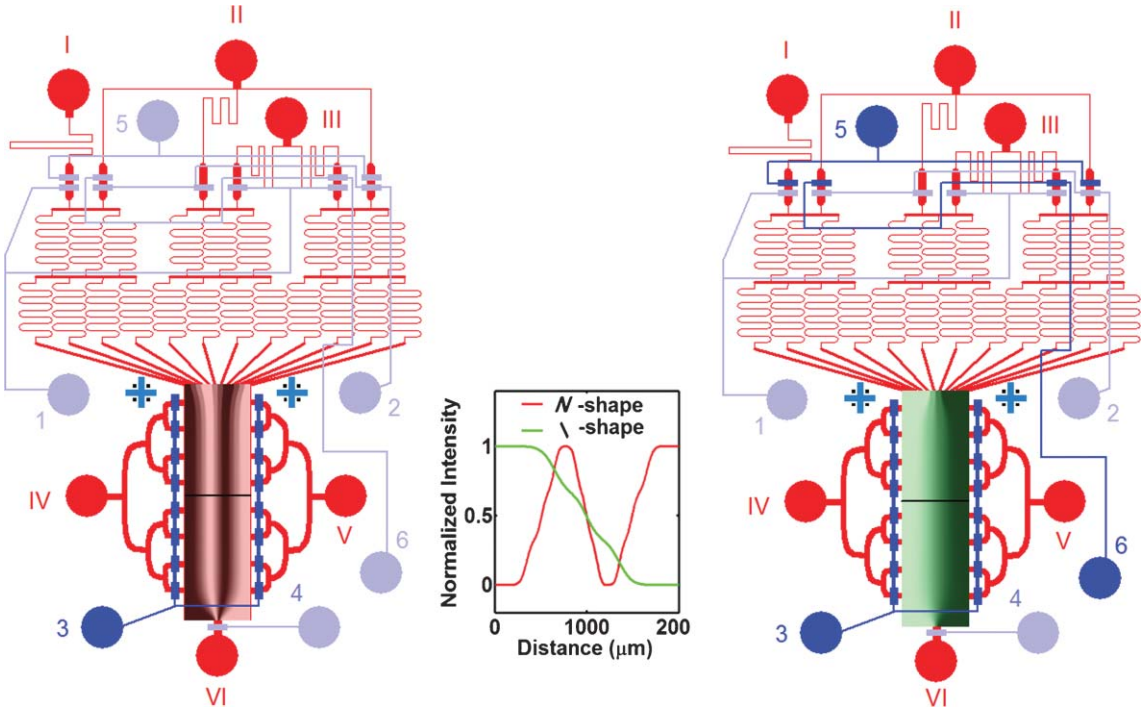

Fig. 2 Functional demonstration of the composite-gradient generator. By connecting inlets I and III to low concentration solutions and inlet II to a high concentration solution, a \- or N-shaped gradient can be generated using the same device through different valve configurations. In the diagrams, the dark blue color illustrates pressurized valves (which stop the fluidic flow beneath) whereas the pale blue color illustrates inactive valves. In the left panel, only valve 3 is turned on and an N-shaped gradient can be generated in the observation chamber. In the right panel, valves 5 and 6 are turned on in addition to valve 3. Therefore, only the middle mixing network is in use and a linear \-shaped gradient is generated. The concentration distributions in the chambers are simulated in FEMLAB using diffusion coefficients of 8.4 $\mu m^2 s^{-1}$ for the N-gradient of laminin and 27 $\mu m^2 s^{-1}$ for the \-gradient of BDNF. The simulated profiles of the two gradients across the chamber are shown in the middle panel.

definitions of initial and turning angles. Since the initial angle of growth cone extension is different for all the growth cones, we chose to track each growth cone for 1 h after the initiation of the BDNF gradient. Based on our experiments, we find that the effect of initial angle on axon turning response diminishes as a function of time and is negligible after 1 hour (data not shown). Only the growth cones that traveled more than 20 μm in the 1 h period were included in the analysis using our custom Matlab code. In the presence of a gradient, the turning angle is defined to be positive if the line indicating the new axonal orientation is directed towards the higher concentration region when compared to the initial direction; otherwise, the angle is negative. In the control experiments, in the absence of a gradient, the turning angle is defined to be positive if the line indicating the new axonal orientation is directed towards the left side with respect to the initial direction; otherwise, the angle is negative. Averages and standard deviations per each analyzed condition were calculated by combining the data from multiple chip experiments. In all the statistical analyses, a two tailed Mann–Whitney test was used for comparison of two groups and the Kruskal–Wallis test for comparing three or more groups unless otherwise noted. Calculations were carried out in GraphPad Prism Version 5 (GraphPad Software, Inc.).

Phase, epifluorescence microscopy

The Alexa 488 gradient and the rhodamine–laminin gradient were imaged wtih a 20× regular working distance objective on a Nikon Diaphot epifluorescence microscope using a 488/512 nm and a 572/628 nm (ex/em) filter set, respectively. Phase-contrast micrographs of axon gradient sensing response was recorded at set intervals with a Nikon TE2000 microscope equipped with a Spot RT camera (Diagnostic Instruments).

Additional methods

Descriptions of the control of valves and fluidic flow in the microfluidic device, actin and microtubule staining and imaging, scanning electron microscopy, and confocal microscopy are available in the ESI.†

Results

Device design and in-chip neuronal culture conditions

A microfluidic device for assaying guidance response of growth cone was designed based on the following requirements: (1) compatibility with neuronal cell culture conditions; (2) capacity to generate sustained, stable and variably shaped integrated gradients of diffusible and surface bound cues; (3) capability to initiate the gradients with high temporal resolution and minimal mechanical disturbance to growth cones; (4) optical accessibility for time lapse imaging of growth cone turning responses and dynamics of fluorescently labeled molecules; (5) the ability to analyze multiple growth cones exposed to diverse conditions in one experiment. The proposed 'composite-gradient generator' satisfying these criteria is

composed of two reversibly-bonded parts (Fig. 1(b)). The first component is a custom microfabricated PDMS chip molded using standard soft lithography techniques[13] (See ESI Fig. 1B†) and the second component is a glass coverslip patterned with micro-wells.

The PDMS chip includes 2 fluidic layers. The bottom fluidic layer (filled with red food-dye in Fig. 1) contains the serpentine mixing network for generating a smooth gradient, a 2 mm by 7 mm chamber for cell culturing and chemotaxis observation, and a symmetrical seeding network that evenly distributes neurons into the observation chamber. The top fluidic layer contains pneumatic control channels (filled with blue food-dye in Fig. 1). When the valve on top of a fluidic channel is pressurized, the membrane constituting the roof of the fluidic channel deflects downward and stops any flow inside the channel. This process is reversible: the channel will regain its connectivity when the control pressure to the valve above is removed. Therefore, by selectively pressurizing/depressurizing specific valves at chosen times, we can control the onset of gradient generation or reconfigure the fluidic connections between the microchannels. As demonstrated schematically in Fig. 2, when solutions with different concentrations of guidance cues are introduced into the device *via* separate inlets, either a \-shaped (or linear) or an N-shaped gradient can be generated in the chemotaxis chamber by selectively opening or sealing off specified channels using the pneumatic control valves. The gradient generated by the continuous convective flow can be maintained at a steady state indefinitely.[14,15]

We found that extending growth cones collapsed rapidly when a moderate flow was produced (see ESI Fig. 2†). This retraction of growth cone is likely to be due to the concomitant shear stress (shear stress = 0.072 dyne cm^{-2}, through a channel of 2 mm (w) by 30 μm (h)). To shield the growth cones from the effects of flow, we etched an array of 100 μm deep parallel micro-wells within the cell culture area on the underlying glass coverslip to selectively increase the chamber height at locations where neurons reside. The fabrication process is described in the ESI (Fig. 3).† The effect of micro-well structure on micro-flow and diffusion was analyzed through mathematical modeling in FEMLAB (COMSOL, see ESI Fig. 4†). The simulation results demonstrated that by increasing the height of neuronal culture environment from 30 μm to 130 μm, the shear stress at the chamber bottom is reduced approximately 16-fold (Fig. 3(a)). We imaged the surface of the micro-wells with scanning electron microscopy (Fig. 3(b)) and verified that the surface of the micro-well was smooth and free from topographical cues that might bias neurite growth.[19,20] The etched coverslips can be easily aligned and bonded to the PDMS component, resulting in the device shown in Fig. 1.

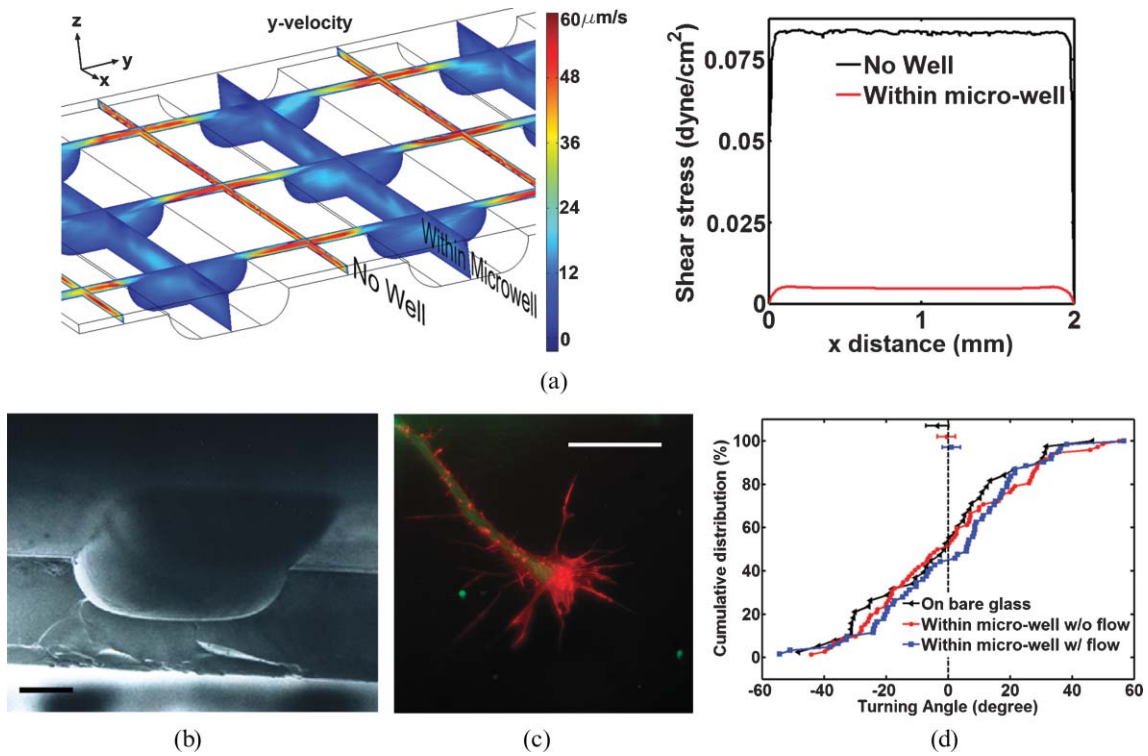

Fig. 3 Initial characterizations of the device. (a) Simulation results demonstrate a significant reduction in flow velocity (left panel) and shear stress (right panel) by incorporating 100 μm deep micro-wells into the observation chamber. The shear stress is measured at 1 μm above the chamber floor or 1 μm above the well bottom. (b) Scanning electronic microscopy images demonstrate a smooth surface on the bottom of the micro-well and a uniform depth of 100 μm. Scale bar: 100 μm. (c) Epifluorescent image of fluorescently-stained actin and tubulin in a growth cone. Neurons within the micro-well are fixed and stained for actin (red) and microtubules (green) with Alexa Fluor 594 Phalloidin and Oregon Green 488 Paclitaxel, respectively. Microtubules are bundled in the axon shaft. Within the growth cone, microtubules are localized to the central domain while actins outline the peripheral zone and reach out to the filopodia. Scale bar: 20 μm. (d) Cumulative distributions of turning angles demonstrate that either the micro-wells or the convective flow (56.7 nL min^{-1}) has no artificial effects on axon growth. The isolated symbols represent mean +/− standard error.

We tested this design by first examining the effects of the well geometry on growth cone guidance in the absence of an active flow. We introduced neurons into the PDL/rhodamine–laminin coated chip and cultured them as described in Methods. Epifluorescent microscopic imaging of the rhodamine–laminin verified the uniformity of laminin coating on the glass surface (see ESI Fig. 5†). The wet-etched glass has preserved its compatibility with high-resolution fluorescent imaging. Shown in Fig. 3(c) is an example of in-chip staining and visualization of actin and microtubule structures within a single growth cone. To confirm that there is no artifactual guidance effect from micro-well walls, we recorded the extension of neurites on either flat glass or in micro-wells for one hour in a static culture environment 6 hours after plating. The cumulative distributions of turning angles suggest that the growth of axons was random and not biased by micro-well structure (Fig. 3(d), average turning angle $-0.5 \pm 2.9^\circ$, $n = 72$ within the micro-well compared to $-3.5 \pm 3.7^\circ$, $n = 38$ on flat glass; two-tailed Mann–Whitney test, $p = 0.7$).

We tested the shear dampening function of micro-wells by culturing neurons on either flat glass or within micro-wells statically for 6 h within PDMS chips and then initiated a convective flow of 56.7 nL min^{-1}. Axons that were cultured on flat glass retracted rapidly when exposed to convective flow (shear stress = 0.072 dyne cm^{-2}, through a channel of 2 mm (w) by 30 μm (h) (see ESI Fig. 2†). In contrast, axons cultured within micro-wells continued their extension during the whole assay period; thereby validating the function of micro-wells for protecting neurons from shear stress. We also found that neurites did not align with the direction of flow (Fig. 3(d), average turning angle $1.1 \pm 2.9^\circ$, $n = 61$ in a flow of 56.7 nL min^{-1} compared with $-0.5 \pm 2.9^\circ$, $n = 72$ without flow; $p = 0.7$), indicating that the convective flow presented in the gradient assay experiments (reported in the upcoming sections) did not bias the extension of growth cones.

Characterization of the integrated gradients of soluble cues and surface-bound cues

We next used the device to generate and characterize composite gradients of two guidance cues. First, the N-shaped gradient of laminin solution was generated using the configuration in the left panel of Fig. 2 (see Methods for details). This gradient was deposited onto the positively charged (PDL-coated) culture surface through non-specific adsorption[12]. Profiles of the substrate-bound rhodamine–laminin were visualized using an epifluorescent microscope (Fig. 4(a)). The adsorbed laminin gradient remained stable on glass surface for the duration of the growth cone turning assay (data not shown). We then switched the inlet solutions and pressurized the valves according to the configuration shown in the right panel of Fig. 2 to generate a linear diffusible BDNF gradient (see Methods for details). Since the neurons in our device would reside in the array of micro-wells, we used confocal imaging to verify that a gradient of a soluble factor at the bottom of the wells would be equal to the gradient at the top of the wells. Purified EGFP was used in the gradient characterizations because it is naturally fluorescent and its diffusion coefficient is similar to that of BDNF. The confocal

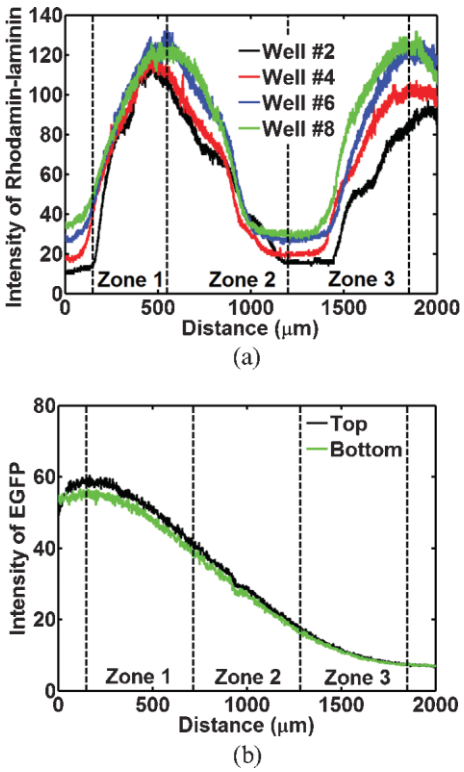

Fig. 4 Characterization of the generation of composite gradients of soluble cues and surface-bound cues. (a) Comparison of N-shaped rhodamine–laminin in different wells. The N-shaped surface-bound rhodamine–laminin gradient across the chamber width is visualized using epifluorescent imaging. The smooth laminin gradient is preserved with small variation in all the micro-wells along the length of the chamber. (b) Comparison of steady state EGFP gradient profiles at the top and bottom of well 4 with a volumetric flow rate of 56.7 nL min^{-1}. EGFP is used as a proxy for BDNF distribution due to the similarity of their molecular weights (29 kD and 27 kD respectively) and thus their diffusion coefficients.

study revealed that a well-defined linear gradient was generated throughout the observation chamber, except for the areas very close to the side walls where the gradient shape was slightly perturbed, most likely due to a wall effect (Fig. 4(b)). Therefore, in the analyses of subsequent assays, growth cones residing in the areas within 150 μm of the two side walls were excluded from consideration.

The difference between the transient time of gradient stabilization between the top and the bottom of the well was very small and beyond the temporal resolution of the instrument we used. The simulation results from FEMLAB suggested that this time difference was less than 20 s (see ESI Fig. 6†). During the ensuing steady state gradient distribution, we found an almost undetectable difference between the gradient profiles at the top and bottom of each well as long as convective flow is maintained (Fig. 4(b)). The profile of gradient varied slightly from the first well to the last well due to passive diffusion (see ESI Fig. 7†). The gradient profile established in the observation chambers could be easily and robustly reproduced in repeated assays as long as the same fluidic flow rate of 56.7 nL min^{-1} was applied. Thus by recording the position of a growth cone within a specific

micro-well and the BDNF concentration in each inlet solution, we could precisely deduce the values and the mean concentration of the BDNF gradient experienced by the target growth cone.

Linear gradient of BDNF induces repulsive turning response in growth cone on a surface with uniform laminin coating

For the first proof-of-concept experiment, we applied the proposed composite-gradient generator to analyze the effect of a linear gradient of BDNF, a known soluble chemotactic cue, on growth cone locomotion. After neurons were plated in the uniformly coated chip for 6 h and started forming neurites, a linear BDNF gradient of 0 to 50 ng mL^{-1} was introduced into the observation chamber. Neurites started responding to the gradient as early as 10 minutes after gradient stimulation. Time lapse imaging showed that the growth cones exhibited marked repulsive turning in response to a linear gradient of BDNF (Fig. 5(a)). This response was statistically significant (p = 0.003), with an average turning angle of $-12.3^\circ \pm 3.3^\circ$ (n = 63) compared to $1.1^\circ \pm 2.9^\circ$ (n = 61) in control experiments. This observation is the first to record unambiguously the guidance response of growth cones to linear BDNF gradients, showing the repulsive directionality consistent with repulsion observed previously for embryonic *Xenopus* retinal neurons in approximately exponential BDNF gradients generated by pipette.[21] The robust result points to another major advantage of our system: the ability to assess the turning behaviors of multiple growth cones in a highly parallel fashion (see ESI Fig. 8† for the montage image of growth cones growing in a microwell). Typically, 10 to 25 neurons are analyzed per chip experiment and at least 3 chip experiments are performed per modulated experimental parameter.

As the slope is constant for a linear gradient, we could examine the dependence of growth cone gradient sensing on the mean concentration of a BDNF gradient. To facilitate analysis, we evenly binned the neurites into 3 groups based on their residing zones in the observation chamber (as in Fig. 4(b)). The BDNF concentration in these three zones was calculated to be around 33–50 ng ml^{-1} in zone 1, 17–33 ng ml^{-1} in zone 2 and 0–17 ng ml^{-1} in zone 3, with each

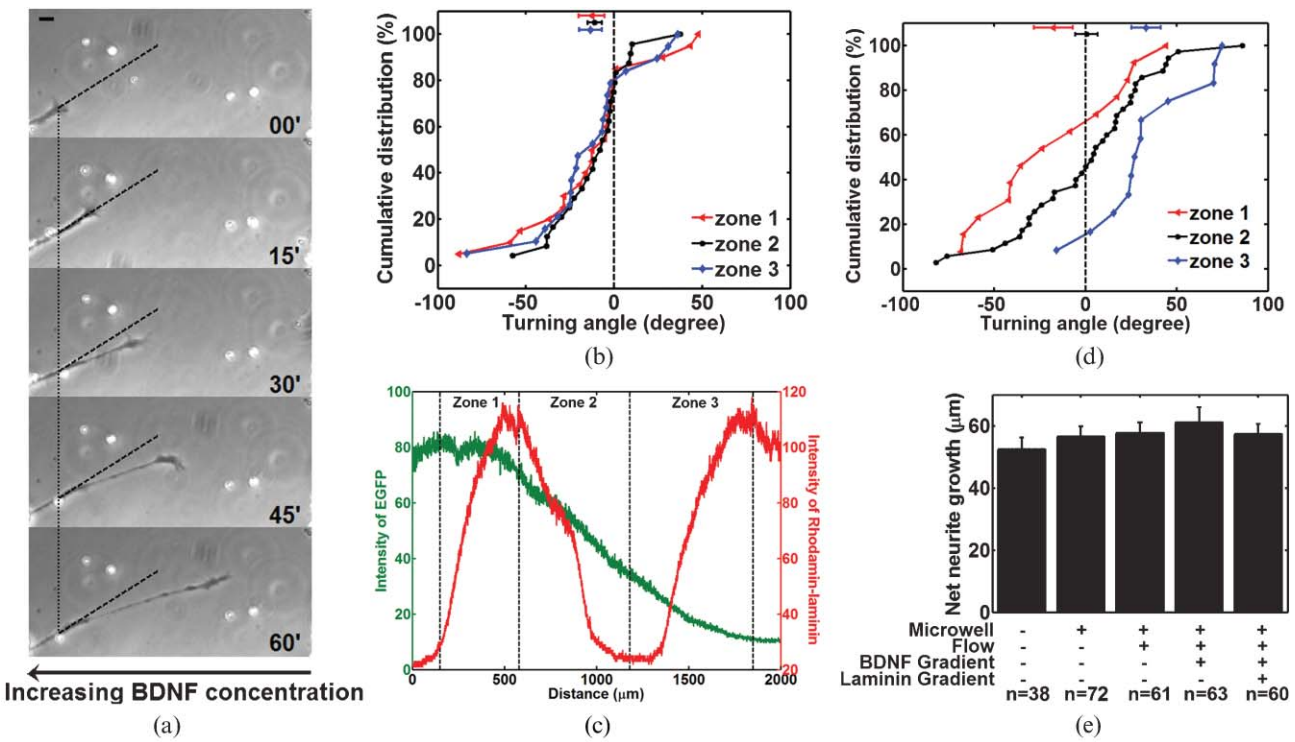

Fig. 5 Growth cone response to single and composite gradients. (a) Representative time-series images illustrate a growth cone turning away from higher concentration of BDNF when it is cultured on uniform laminin surface. (b) In the three zones with different mean concentrations of the linear BDNF gradient, growth cones exhibit similar repulsive responses when the underlying laminin coating is uniform (Kruskal–Wallis test, p = 0.8). (c) A linear BDNF gradient is superimposed on a surface-bound N-shaped rhodamine–laminin gradient. The profile shown is from the fifth micro-well of the observation chamber. The BDNF gradient is measured indirectly by measuring the concomitantly administrated EGFP distribution in a confocal fluorescent setting. (d) The cumulative distributions of turning angles to composite BDNF and laminin gradients at the end of a 1 h assay in the three zones of the chamber. The polarity of the turning angle is defined with respect to the direction of the BDNF gradient: positive when turning to the higher concentration of BDNF and negative when turning to the lower concentration of BDNF. In zone 1, growth cones are repelled by BDNF and extend up the laminin gradient; in zone 2, growth cones show no preferred turning; in zone 3, growth cones are attracted by BDNF and extend down the laminin gradient. The isolated symbols represent mean +/− standard error. In comparison to (b), this figure demonstrates that polarity of growth cone guidance is synergistically regulated by combined gradients of BDNF and laminin and finely tuned by the mean concentration of BDNF gradient. (e) Putative mechanical cues (micro-well structure, convective flow) or introduced chemical cues (gradients of BDNF and laminin) do not affect the speed of neurite extension (Kruskal–Wallis test, p = 0.8). The error bar represents standard error.

zone extending over approximately 570 μm. We found that growth cones in all three zones responded similarly to the BDNF gradient (Kruskal–Wallis test, $p = 0.8$), with the average turning angles for growth cones in zone 1, 2 and 3 being $-12.7 \pm 7.2^\circ$ ($n = 20$), $-11.0 \pm 4.1^\circ$ ($n = 24$), and $-13.4 \pm 6.4^\circ$ ($n = 19$), respectively (Fig. 5(b)). These results suggest that, when the absolute BDNF concentration is within the range of 0–50 ng mL^{-1}, growth cones sense a concentration difference, but not the average concentration value. This result is especially meaningful, since the range of the BDNF concentrations was expected to span almost completely the sensitivity range for the receptor activation, with the highest concentration used, 50 ng mL^{-1} (or 1.85×10^{-9} M) being close to the dissociation constant of BDNF with respect to its receptor, measured at 1.3×10^{-9} M by Rodrigeuz-Tear and Barde.[22] This result suggested that growth cones could adapt to changing average BDNF concentration during migration. Furthermore, it also suggested that the gradient sensing of growth cones was equally precise for a wide range of fractional gradient values (spanning from 0.5% in zone 1 to 6% in zone 3). Fractional gradient values are a common metric of gradient sensitivity, being defined as the concentration difference between the front and back of a growth cone (estimated as 10 μm in width) relative to its midpoint concentration.

The polarity of growth cone guidance is synergistically regulated by composite BDNF and laminin gradients

In developing and regenerating neural tissues, migrating growth cones are often guided by combinations of soluble and substratum-bound cues. However, previous efforts only investigated independent pathfinding responses to either soluble[3–6] or extracellular matrix cues[11,12,23] due to the limitations of the gradient generating methods used. A key advantage of the composite-gradient generator is that one can reliably and reproducibly generate precisely aligned combinational gradients of diffusible and substratum-bound guidance cues with minimal perturbation to growth cones. We thus utilized this device to investigate how growth cone guidance is synergistically regulated by combined soluble linear BDNF and surface-bound N-shaped laminin gradients.

After neurons were cultured on the N-shaped laminin gradient for 6 h and formed neurites, we measured the initial angle of axon extension at the end of the 6 h culture. We found that, when cultured on a linear laminin gradient of 30 ng mL^{-1} mm^{-1}, $61.5 \pm 3.6\%$ axons ($n = 182$) extended towards the higher laminin concentration. In contrast, when cultured on a uniform laminin coating, $50.2 \pm 3.2\%$ axons extended toward one side and $49.8 \pm 3.2\%$ toward the other ($n = 234$). These results suggest that axons from *Xenopus* spinal neurons were attracted to higher concentrations of laminin ($p = 0.02$), consistent with previous findings with rat hippocampal neurons[12] and chick embryonic DRG neurons[11].

A linear BDNF gradient was then initiated, exposing the growth cones to both diffusible and surface-bound gradients, as shown in Fig. 5(c). The observation chamber was subsequently divided into 3 zones according to the polarity of the laminin gradient. In Fig. 5(d), we showed the cumulative distributions of the turning angles at the end of a one-hour assay among the growth cones in the three zones (the polarity of turning angle is defined with regard to BDNF gradient). The growth cones in zone 2 were exposed to conflicting turning signal, and exhibited virtually unbiased stochastic turning responses (average turning angle $0.6 \pm 6.1^\circ$, $n = 35$; $p = 0.92$), indicating a lack of prioritization in their responses to laminin *vs.* BDNF. In both zones 1 and 3, the gradients were in opposite orientation with respect to each other. Growth cones in zone 1 exhibited the expected response equivalent to both repulsion in the BDNF gradient and attraction to the laminin gradient ($-17.6 \pm 10.6^\circ$, $n = 13$; Mann–Whitney test, one-tailed, $p = 0.05$). Surprisingly, counter to the expectation that response would be similar to that in zone 1, in zone 3 the growth cone response was converted to attraction to BDNF, and respectively repulsion to the laminin gradient ($33.2 \pm 8.0^\circ$, $n = 12$; Mann–Whitney test, $p = 0.002$). We note that the observed different turning responses were not due to a change of growth cone extension rate under varied conditions (Fig. 5(e)). Since the device allowed us to investigate growth cone responses to the three different combinations of gradients simultaneously, a batch-to-batch difference in experimental settings was also an unlikely explanation for our surprising observation. The only difference in the imposed guidance cues between zones 1 and 3 was the mean concentration of the BDNF gradient. Overall, the results suggest that when growth cone is presented with opposing gradients of BDNF and laminin, the polarity of guidance response of a growth can be modulated by manipulating the mean concentration of BDNF gradient.

Discussion

Elucidating the cellular and molecular mechanisms underlying growth cone guidance can aid in the prevention of developmental disorders of the nervous system such as mental retardation, dyslexia and cerebral palsy. Furthermore, select populations who suffer from neurodegeneration following injury, stroke or deleterious disease will benefit from a better understanding of growth cone guidance during nerve regeneration. The application of *in vitro* assaying systems has considerably facilitated exploration of these areas of research. This report describes a novel growth cone turning assay for investigating the guidance response of growth cone to various integrated gradients of diffusible and surface-bound cues. The proposed experimental platform is a flexible tool that can more faithfully recapitulate the complexity of the *in vivo* guidance conditions.

Gradients generated in microfluidic devices can be stably maintained for long periods of time. Moreover, the slope and average concentration of the gradient can be individually modulated, allowing independent analysis of the roles of these parameters. Recent work by Millet *et al.*[24] has rigorously demonstrated that monomer extracted PDMS exhibits low neurotoxicity for long-term neuronal culture in microfluidic devices. However, the inherent presence of microflows in many microfluidic gradient generators has severely limited application of microfluidic technologies to neurons due to their shear-sensitivity. Shear stress reduction—one of the critical features of the presented device—was necessitated by the strong

retraction of growth cones in fluidic flow. Shear stress at the floor of a fluidic channel is linearly dependent on volumetric flow rate and inverse square dependent on channel height. Therefore, to reduce shear stress, one could either decrease the volumetric flow rate through lowering the driving pressure differential or increase the height of the chamber where the cells reside. Although both strategies are potentially viable, the former one presents several difficulties in terms of the gradient development due to the associated decrease in flow velocity. A decrease in the flow velocity would increase the time for the fluid stream to travel from the beginning to the end of the observation chamber. This increase in traveling time will have two undesirable effects. First, it will prolong the time it takes for a steady state gradient to form. However, the transient stage of gradient development should not exceed the response onset-time of axon turning, which is around 5–10 minutes.[25] Second, it will result in an increase in the residence time and therefore lead to rapid gradient dissipation, causing the value of the gradient to vary considerably throughout the length of the observation chamber. If, alternatively, the shear stress is reduced by increasing the height of the chamber, the volumetric flow rate would not be strongly affected when the driving pressure differential is unchanged. Based on this analysis, we incorporated an array of micro-well structures within the cell culture chamber. Their depth of 100 μm fully protected neurons from shear stress during turning assays.

We have implemented other methods of micro-well fabrications and evaluated their practicality as well (data not shown). They include (1) SU8-2100 layer with lithographically defined micro-wells[26] and (2) PDMS stencil and glass-bottom composite micro-wells.[27,28] We found that SU-8 microwells on glass can only be robustly sealed to a PDMS device by oxygen plasma treatment. Since this particular method forms an irreversible bond, the PDMS device and the sealing bottom cannot be separated for cleaning, the device can only be used once. Microwells constructed from PDMS stencil and glass-bottom composite encounters similar limitation. This one-time use limitation puts high premium on fabrication time, and is the major consideration that drove us to etch microwell directly onto the glass coverslip. Glass micro-well does not introduce any complication to the regular microfluidic chip users, as well as allowing multiple usages of the fabricated chip.

Another powerful feature incorporated into the composite-gradient generator is the pneumatic membrane valves[13] for controlling the onset and shape of gradients. On-chip valves allow precise initiation of flow, thus minimally perturbing the localization and well-being of neurons. The topology of the fluidic networks can be reconfigured by pressurizing selected valves, permitting superimposition of gradients with different spatial profiles in perfect registration without the need for re-aligning to a separate device. The fluidic network design can also be easily expanded to allow analysis of a variety of combinations of graded stimuli.

In this study, we demonstrated how the proposed device can be used to investigate the sensitivity of growth cone gradient sensing to the mean concentration of the guidance cue. In addition to demonstrating the ability of growth cones to turn in response to linear gradients, our analysis showed that the turning responses, which is a downstream manifestation of the gradient sensing capability, exhibited no dependence on the mean BDNF concentration of the gradient in the ranges tested (Fig. 5(b)). We thus can infer that the molecular circuitry for gradient sensing intrinsic to growth cone is capable of filtering out the background average concentration, and detect only the absolute difference in spatial concentration. This property is commonly termed ''adaptation'', referring to the property of the signaling network to adapt to persistent stimulation by always reverting back to the baseline. Consequently, adaptation could confer onto neurons the ability to optimally sense gradients within a wide range of BDNF concentration, allowing the growth cones to be precisely guided over long distances along the gradient.

We applied the composite-gradients generator to investigate, for the first time, the sensitivity of growth cone responses to integrated gradients of soluble and surface-bound cues. When the concentration gradients of BDNF and laminin were presented together in the same direction, we found that the conflicting signals resulted in random turning of growth cones. This finding indirectly suggests that growth cones do not prioritize BDNF over laminin cues, or *vice versa*. Furthermore, we observed that the polarity of growth cone responses to opposing BDNF and laminin gradients is modulated by the average BDNF concentration. Our results support the hypothesis that a single guidance cue is able to elicit multiple types of turning responses from the growth cone, with the outcome dependent on the cellular-context. Based on the observations reported in this article, in Fig. 6(a) we illustrate the scenarios in which combined BDNF and laminin gradients can modulate axon position within a certain proximity to areas with high (or low) BDNF/laminin concentration. Manipulating the mean BDNF concentration and relative direction of the two gradients therefore provide the possible means for limited numbers of guidance cues to not only control the migration direction of growth cones but also to specify their topographical positions during the development.

Multiple guidance cues are coordinated by the modulation of intracellular signaling events. A possible mediator of the growth cone behavior described above is intracellular cAMP, whose production could be negatively regulated by either BDNF or laminin in a dose-dependent fashion (Fig. 6(b)).[21,29] Intracellular cAMP levels are known to modulate the polarity of growth cone guidance:[5] when [cAMP] is above a threshold, a BDNF gradient triggers attraction; otherwise, repulsion.[25] In our experimental setting where the laminin coating concentration is uniformly high in three adjacent zones of the gradient field, the growth cones could have [cAMP] below the threshold. However, the growth cones in zone 3 would have a conceivably higher cAMP than those in zone 1 because the mean concentration of BDNF gradient was lower (Fig. 6(b), blue curve). It is plausible that the intracellular [cAMP] in zone 3 can be very close to the switching threshold. Therefore, when the concentration of another negative regulator of cAMP, laminin, decreases, [cAMP] can increase further and finally exceed the switching threshold, causing the observed conversion from repulsion to attraction in the experiments with graded laminin (Fig. 6(b), magenta curve). The composite-gradient generator is highly compatible with high-resolution live-cell fluorescent imaging, which will greatly facilitate the

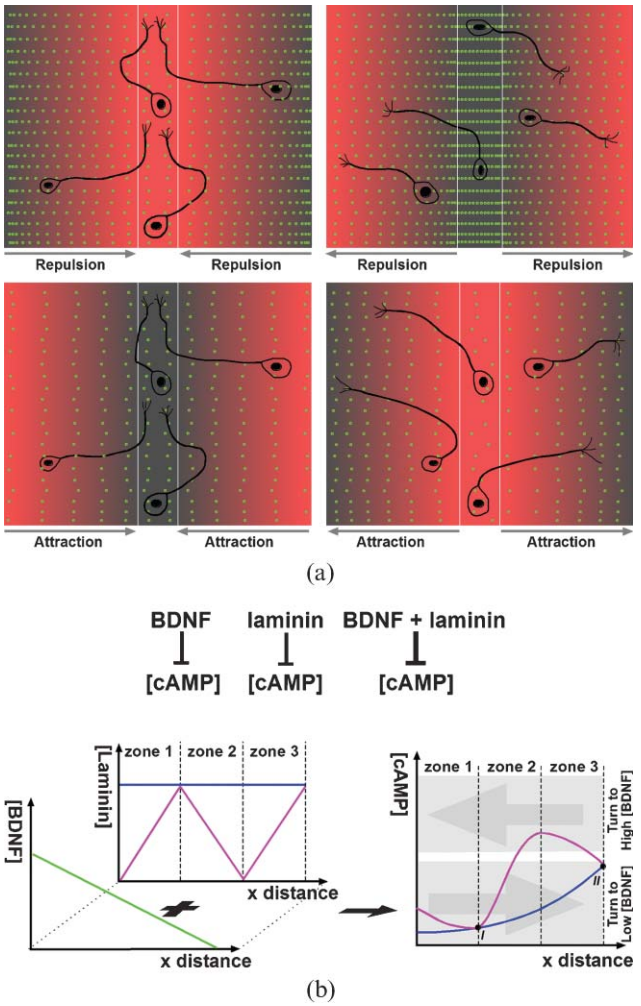

Fig. 6 Conceptual illustration of how coordinated BDNF and laminin signals modulate axon position within a certain proximity to areas with high (or low) laminin concentration and how they achieve this versatility through the regulation of intracellular [cAMP]. (a) Combined BDNF and laminin gradients can control axon extension in various ways by manipulating the mean concentration of BDNF gradient and relative directions of BDNF and laminin gradients. In this illustration, the intensity of red background represents the concentration of surface-bound laminin; the density of green dots represents the concentration of soluble BDNF. Upper panels: when laminin gradient is combined with BDNF gradient with high mean concentration, axons can be confined to an area with high laminin concentration (left) and kept outside of an area with low laminin concentration (right); Lower panels: when laminin gradient is combined with BDNF gradient with low mean concentration, axons can be confined to an area with low laminin concentration (left) and kept outside of an area with high laminin concentration (right). (b) BDNF and laminin can independently exert a negative effect on the production of intracellular cAMP, and may have a synergistic effect when they are combined. On a uniform laminin surface (indicated by the blue curve), low concentration of BDNF exerts less negative effect on the production of cAMP, hence leading to a higher [cAMP] in the growth cones in zone 3. The [cAMP] is potentially very close to the switching threshold, which determines the polarity of the turning response of growth cones to the BDNF gradient. Decreasing the concentration of laminin, as in the N-shaped gradient case (illustrated in magenta), may allow the [cAMP] to rise above the switching threshold, explaining why we have observed the attractive turning response to BDNF for neurons in zone 3.

elucidation of the underlying molecular mechanisms of neuron chemotaxis, *e.g.*, monitoring intracellular cAMP level in real-time within single growth cones using published cAMP FRET probes.[30–32] Overall, the behavior of growth cones in the combined gradients is illustrative of the power of the proposed assay system to generate new hypotheses that can guide further research into the guidance principles and mechanisms.

Conclusions

We anticipate that future experiments with this device will include expanding the range of imposed BDNF gradient, exploring combinatorial gradients of other moieties, and monitoring the spatiotemporal kinetics of intracellular molecules during growth cone turning. Combined with the ability to stably hold or dynamically switch the gradient, the reported device holds great promise for investigating a host of questions related to nervous system development and regeneration.

Acknowledgements

This work was funded in part by the seed awards from the Institute for Nano-Biotechnology and Institute for Cell Engineering at the Johns Hopkins University to A. L. NIH, March of Dimes, Klingenstein Fellowship Award in Neuroscience, Alfred P. Sloan Foundation and Adelson Medical Research Foundation provided support to G.L.M. The authors wish to thank Julie S. McGurk for providing *Xenopus* embryos; Alex Groisman and Nick Gaiano as well as anonymous reviewers for helpful remarks.

References

1 M. Tessier-Lavigne and C. S. Goodman, *Science*, 1996, **274**, 1123–1133.
2 B. K. Mueller, *Annu. Rev. Neurosci.*, 1999, **22**, 351–388.
3 A. Lohof, M. Quillan, Y. Dan and M. Poo, *J. Neurosci.*, 1992, **12**, 1253–1261.
4 J. Q. Zheng, M.-m. Poo and J. A. Connor, *Perspect. Dev. Neurobiol.*, 1996, **4**, 205–213.
5 H.-j. Song, G.-l. Ming and M.-m. Poo, *Nature*, 1997, **388**, 275–279.
6 G.-l. Ming, S. T. Wong, J. Henley, X.-b. Yuan, H.-j. Song, N. C. Spitzer and M.-m. Poo, *Nature*, 2002, **417**, 411–418.
7 M. Nishiyama, A. Hoshino', L. Tsai, J. R. Henley, Y. Goshima, M. Tessier-lavigne, M.-m. Poo and K. Hong, *Nature*, 2003, **423**, 990–995.
8 W. J. Rosoff, J. S. Urbach, M. A. Esrick, R. G. McAllister, L. J. Richards and G. J. Goodhill, *Nat. Neurosci.*, 2004, **7**, 678–682.
9 P. Clark, S. Britland and P. Connolly, *J. Cell Sci.*, 1993, **105**, 203–212.
10 C. Weinl, U. Drescher, S. Lang, F. Bonhoeffer and J. Loschinger, *Development*, 2003, **130**, 1635–1643.
11 D. N. Adams, E. Y.-C. Kao, C. L. Hypolite, M. D. Distefano, W.-S. Hu and P. C. Letourneau, *J. Neurobiol.*, 2004, **62**, 134–147.
12 S. K. W. Dertinger, X. Jiang, Z. Li, V. N. Murthy and G. M. Whitesides, *Proc. Natl. Acad. Sci. U. S. A.*, 2002, **99**, 12542–12547.
13 M. A. Unger, H.-P. Chou, T. Thorsen, A. Scherer and S. R. Quake, *Science*, 2000, **288**, 113–116.
14 N. L. Jeon, S. K. W. Dertinger, D. T. Chiu, I. S. Choi, A. D. Stroock and G. M. Whitesides, *Langmuir*, 2000, **16**, 8311–8316.
15 S. K. W. Dertinger, D. T. Chiu, N. L. Jeon and G. M. Whitesides, *Anal. Chem.*, 2001, **73**, 1240–1246.
16 N. L. Jeon, H. Baskaran, S. K. W. Dertinger, G. M. Whitesides, L. V. D. Water and M. Toner, *Nat. Biotechnol.*, 2002, **20**, 826–830.

17 S. Paliwal, P. A. Iglesias, K. Campbell, Z. Hilioti, A. Groisman and A. Levchenko, *Nature*, 2007, **446**, 46–51.
18 N. Tabti, J. Alder and M.-M. Poo, in *Culturing Nerve Cells*, ed. G. Banker and K. Goslin, MIT Press, Cambridge, Massachusetts, 2nd edn, 1998, pp. 237–260.
19 A. M. Rajnicek, S. Britland and C. D. McCaig, *J. Cell Sci.*, 1997, **110**, 2905–2913.
20 N. M. Dowell-Mesfin, M.-A. Abdul-Karim, A. M. P. Turner, S. Schanz, H. G. Craighead, B. Roysam, J. N. Turner and W. Shain, *J. Neural Eng.*, 2004, **1**, 78–90.
21 V. H. Hopker, D. Shewan, M. Tessier-Lavigne, M.-m. Poo and C. Holt, *Nature*, 1999, **401**, 69–73.
22 A. Rodrigeuz-Tear and Y.-A. Barde, *J. Neurosci.*, 1988, **8**, 3337–3342.
23 A. C. v. Philipsborn, S. Lang, J. Loeschinger, A. Bernard, C. David, D. Lehnert, F. Bonhoeffer and M. Bastmeyer, *Development*, 2006, **133**, 2487–2495.
24 L. J. Millet, M. E. Stewart, J. V. Sweedler, R. G. Nuzzo and M. U. Gillette, *Lab Chip*, 2007, **7**, 987–994.
25 G.-l. Ming, H.-j. Song, B. Berninger, C. E. Holt, M. Tessier-Lavigne and M.-m. Poo, *Neuron*, 1997, **19**, 1225–1235.
26 V. I. Chin, P. Taupin, S. Sanga, J. Scheel, F. H. Gage and S. N. Bhatia, *Biotechnol. Bioeng.*, 2004, **88**, 399–415.
27 C. J. Wang, A. Bergmann and A. Levchenko, *Nature Biotechnology Winter Symposia: Signal Transduction in Cancer, Miami*, 2005.
28 E. Ostuni, R. Kane, C. S. Chen, D. E. Ingber and G. M. Whitesides, *Langmuir*, 2000, **16**, 7811–7819.
29 Q. Wang and J. Q. Zheng, *J. Neurosci.*, 1998, **18**, 4973–4984.
30 Y. V. Gorbunova and N. C. Spitzer, *Nature*, 2002, **418**, 93–96.
31 L. M. Dipilato, X. Cheng and J. Zhang, *Proc. Natl. Acad. Sci. U. S. A.*, 2004, **101**, 16513–16518.
32 V. O. Nikolaev, M. Bunemann, L. Hein, A. Hannawacker and M. J. Lohse, *J. Biol. Chem.*, 2004, **279**, 37215–37218.